

# Zero-Bias Anomalies and g-factors in Atomic-Scale Gold Contacts

A. Anaya, A. L. Korotkov, M. Bowman, and D. Davidovic,\*  
Georgia Institute of Technology, Atlanta, GA 30332  
(Dated: May 21, 2019)

We measure electron transport in atomic-scale gold point contacts, at the crossover from tunneling into metallic conduction. At milli-Kelvin temperature, we observe a zero-bias anomaly in contact conductance, which is a precursor to a tunneling gap. The anomalous conductance exhibits nonmonotonic dependences with magnetic field and energy, reflecting an addition of Zeeman energy and kinetic energy. Surprisingly, g-factors  $2.0 \pm 0.4$  differ greatly from g-factors of isolated gold grains. Our g-factors are consistent with distribution of g-factors in bulk, while electronic diffusion indicates strong spin-orbit scattering.

Zero-bias anomalies (ZBA) in the tunneling spectra of macroscopic junctions have been known for many years. Some of the ZBAs have been explained, for example Altshuler and Aronov have found that many ZBAs are a precursor to the metal insulator transition in weakly disordered leads [1]. Some other ZBAs have not been completely understood, for example a so called "giant resistance peak" [2].

In this work, as a preliminary investigation, we find similar ZBAs in atomic-scale contacts between weakly disordered metals. Unlike the ZBAs in macroscopic junctions, the ZBAs in atomic scale contacts exhibit non-monotonic dependences with magnetic field. The conductance versus magnetic field and voltage suggest that the nonmonotonic dependence is due to addition of Zeeman energy and kinetic energy, resembling the addition spectra of quantum dots. The applied magnetic field ( $H$ ) changes the kinetic energy of electrons at the Fermi energy, by the Zeeman splitting. In response, wavefunctions of different kinetic energies extend through the contact at the Fermi energy.

All our samples have been exposed to air before cooling to low temperatures. It's important to understand atomic conduction in non-ideal situations, if such conduction is to be used in practical devices. Adsorbates from air or poor vacuum introduce complication in exact interpretations of transport properties at low temperatures. However, these complications can, in principle, be surmounted by the application of a statistical approach, for example the random matrix theory. Besides, with some particular realizations of disorder, new physical phenomena in quantum transport can arise, that may not be found in clean contacts.

As we discuss below, exposure to air makes our samples very different from the ballistic atomic-scale contacts studied before. Until now, electron transport in atomic-scale contacts at low temperatures has been studied by break-junctions and scanning tunneling microscope (see Ref. [3] and refs therein).

Many experiments [3] show that if the wire is broken at low temperatures in ultra-high vacuum, then break-junction contacts will be ballistic. The conductance fluctuations (CF) measurements by Ludoph *et al.* [4] in gold

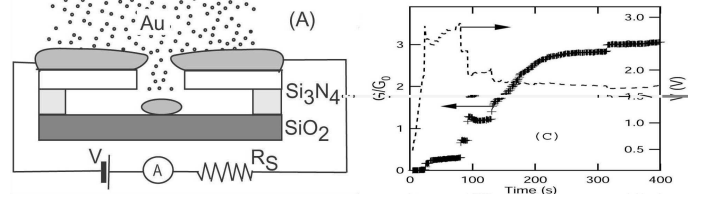


FIG. 1: A. Schematic of sample preparation. B. Conductance versus time and sample bias versus time during electromigration.

break junctions at 4.2K find that the CF amplitude is greatly suppressed from the universal value,  $\sim e^2/h$ . The suppression occurs because only one, out of many conduction channels, is partially open, since completely open conduction channels contribute weakly to CF. [4, 5, 6]

We are not aware of reports on the ZBA in atomic scale contacts. The ZBA is not the only difference between our samples and ballistic break junctions. For example, the characteristic energy scale of CF in our samples is three orders of magnitude smaller than the same in ballistic break junctions, and our fluctuation amplitude approaches the universal value. Many of these differences can be explained by the impurities in our samples, which render the channels diffusive. Numerical simulations by Maslov *et al.* [5] confirm this assumption, finding that when conduction channels of the contacts are partially open, then conductance fluctuations almost reach the levels of conductance fluctuations in the leads.

We prepare gold contacts at room temperature by electromigration. The details of sample fabrication is available in Ref [7]. To summarize, a pure gold film is deposited onto two insulating  $Si_3N_4$  substrates separated by a 70 nm slit, as shown in Fig. 1-(A), in a pressure of  $1 \times 10^{-7}$  torr. Electric current across the slit is monitored during deposition, while protrusions from the bulk extend into the slit and reach corresponding protrusions on the other side of the slit. Samples are placed in series with an external resistor  $R_S$  which is varied from 8 – 20k $\Omega$ , and the applied voltage is varied from 0 – 10V.

When tunneling current is detected, an atomic scale gap separates a pair of protrusions, and then we stop

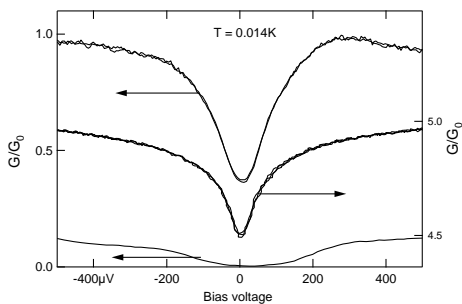


FIG. 2: A. Zero-bias conductance peaks of three samples.

metal deposition. Electromigration pulls the protrusions closer together, increasing the tunneling conductance  $G$ . When  $G > 1/R_S$ , the voltage drop across the sample decreases by voltage division, changing the voltage source into a current source, and electromigration stops. This process creates atomic-scale contacts of high stability. Figure 1-B shows conductance  $I/V_{sample}$  traced as a function of time, by sweeping the applied voltage from zero to  $\sim 5V$ , with a series resistor of  $8.25k\Omega$ . Also shown is the voltage drop across the contact  $V_{sample}$ , illustrating voltage division.

The conductance trace contrasts our samples with ballistic gold break-junctions [3], where the first conductance step is found to be close to  $1G_0 = 2e^2/h$ . We suggest that the adsorption of impurities like water on gold surfaces during electromigration is a likely cause of smaller conductance steps than  $G_0$ .

The samples are annealed at room temperature for days, and then they are slowly cooled to cryogenic temperatures, at a rate of  $\sim 10K/hour$ . The base electronic temperature is ultra-low,  $T_{electron} \leq 0.05K$ , using standard cryogenic filtering techniques. Low electronic temperature is essential, because the ZBAs are rounded at least by  $k_B T$ . In some of our samples, there are ZBAs that completely wash out at  $0.2K$ . In transport measurements, the applied voltage is a sum of a constant part and an AC voltage with amplitude  $2\mu V$ . Conductance is measured by lock-in detection with an accuracy better than 1%.

The ZBAs of three samples are shown in Fig. 2. At higher temperatures, the ZBA peak is diminished. If the high temperature conductance  $G^*$  is larger than  $G_0$ , the depth of the ZBA peak at low temperatures is  $\sim 0.5G_0$  and independent on  $G^*$ . When  $G^*$  is below approximately  $0.5G_0$ , a gap in the tunneling probability appears at low temperature. The ZBAs of contacts with high conductance are precursors to this gap. The tunneling gap, once it is formed, depends strongly on  $G^*$  (not shown).

Since the tunneling gap occurs as  $G^*$  crosses over  $G_0$ , this behavior is suggestive of the Coulomb blockade of small metallic islands or junctions. However, the gap that we measure in atomic-scale junctions is distinct from the

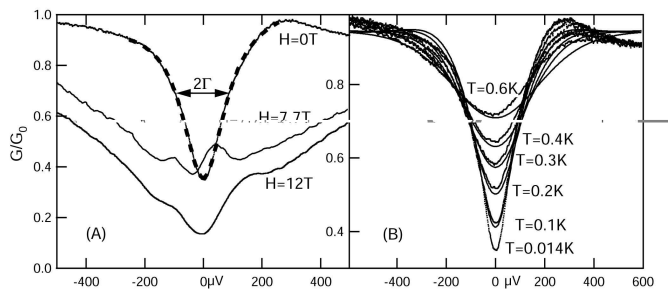


FIG. 3: A. Zero-bias conductance peaks of the selected sample. Dashed line is the best fit to a Lorentzian:  $A + BV + C/(1 + V^2/\Gamma^2)$ . B. Temperature dependence of the zero-bias peak in zero magnetic field. Dots are data, and lines are obtained as described in the text.

Coulomb blockade, in that the size of the gap is strongly dependent on  $G^*$ , even when  $G^* \ll G_0$ .

We select a typical sample, from more than 20 measured samples at  $T = 0.014K$ , within the range of conductance slightly below  $G_0$ . The gold purity used in this sample is 99.99% and there is no Chromium underlayer. The ZBA peak of the sample is shown in Fig. 3-A. The peak fits well to a Lorentzian. The width of the ZBA peak is  $\Gamma \approx 90\mu V$ . We have recently determined that magnetic impurities in this sample are in part responsible for the rounding of the ZBA-peak. An intrinsic linewidth  $\Gamma$  is helpful in analysis of the temperature dependence, as described next.

ZBAs are strongly temperature dependent at low temperatures, as displayed in Fig. 3-(B). In zero magnetic field, the ZBA peak is highly symmetric. The symmetric ZBA peak reflects a suppression in tunneling probability between the leads, which can be shown from the temperature dependence of the ZBA peak. We compare  $G(V, T)$  with a formula for tunneling conductance [1],

$$\frac{G(V, T)}{G_0} = \int \frac{edET(E)}{8k_B T} \left( \frac{1}{\cosh^2 \frac{E-eV/2}{2k_B T}} + \frac{1}{\cosh^2 \frac{E+eV/2}{2k_B T}} \right). \quad (1)$$

This expression neglects temperature and voltage dependences of the transmission probability  $T(E)$ . Temperature dependence come from an anomalous suppression in the density of states in the leads, as a precursor to the metal-insulator transition [1]. Voltage dependence arises from the fluctuations of the metallic conductance [8].

The half-width of the kernel in Eq. 1 is much smaller than  $\Gamma$  if  $T \ll 0.3K$ . Thus, at  $T = 0.014K$ , we approximate the kernel with delta functions, to obtain a relation between  $T(E)$  and  $G(V, 0.014K)$ . Then, using  $T(E)$  determined in this way, we obtain  $G(V, T)$  at higher temperature by Eq. 1. Full lines in Fig. 3-(B) are convolved transmission probabilities by Eq. 1, at temperatures corresponding to the data. The agreement between the data

and the tunneling formula Eq. 1 is very good at zero bias voltage.

This agreement shows that the symmetric ZBA peak at  $H = 0$  reflects a suppression in the tunneling probability through the contact. The absence of temperature dependence in  $T(E)$  shows that the density of states in the leads is not anomalous and the leads are good metals.

The peak in  $T(E)$  in formula 1 occurs at  $E = 0$ .  $E$  in Eq. 1 is measured relative to the average chemical potential between the leads. Thermal broadening in voltage has a full width of  $7k_B T/e$ , which is two times larger than the Fermi full-width of  $3.5k_B T/e$ . This suggests that the suppression in tunneling probability is related to a spatially localized interaction, at the point where the voltage drop is 50%. We speculate that  $T(E)$  suppression at  $E = 0$  is caused by an enhancement of local electron-electron repulsion.

A closer look at Fig. 3 reveals an asymmetric component in conductance versus voltage. Applying a magnetic field  $H$  enhances the asymmetry. For example, at  $H = 7.7T$ , the symmetric ZBA peak nearly vanishes, and the asymmetric conductance is larger than the symmetric ZBA peak. At  $H = 12T$ , the symmetric ZBA peak partially recovers.

Figure 4-A displays conductance versus magnetic field at fixed bias voltage  $V$ . Only near zero bias voltage, does conductance  $G(V, H)$  display pronounced fluctuations. The characteristic field scale of the nonmonotonic conductance fluctuations, at zero bias voltage, is  $1T$ . The fluctuation amplitude is  $\sim 0.3G_0$  peak-to-peak, and it decreases rapidly with voltage. We will return to the fluctuations after discussing a background signal.

$G(V, H)$  in this sample has a pronounced negative magnetoconductance background. This is particularly clear in Fig. 4-A for voltages  $|V| \gg \Gamma$ . Negative magnetoconductance is a signature of weak localization (WL) with strong spin-orbit (SO) scattering.

In Fig. 4B we show a DC conductance  $G_{DC}(V, H)$  versus magnetic field at  $450\mu V$  bias voltage.  $G_{DC}(V, H)$  is obtained by averaging individual  $G(V, H)$  traces within the voltage interval  $[-V, V]$ :  $G_{DC}(V, H) = (I(V, H) - I(-V, H))/2V$ , where  $I$  is the current at bias voltage  $V$ . Averaging in voltage range  $[-450\mu V, 450\mu V]$  results in a perfectly smooth curve displayed in Fig. 4B. The characteristic magnetic field that suppresses SO scattering is  $H_{SO} = 6T$ .

Among all samples measured at low temperature, this is the only sample where  $G_{DC}(V, H)$  flattens near  $H = 12T$  (if  $V$  is sufficiently large to wash out the fluctuating conductance). In this sample,  $12T$  is sufficiently large to completely suppress the interference contributions from SO-scattering. We define the weak localization amplitude as  $\delta G_{WL}(V) = G_{DC}(V, 0T) - G_{DC}(V, 12T)$ . The value of WL amplitude  $\delta G_{WL}(V)$  is decreasing with increasing  $V$ .  $\delta G_{WL}(450\mu V) = 0.45G_0$  is close to the value within the maximum entropy model,  $0.5G_0$  [6, 9] [15].

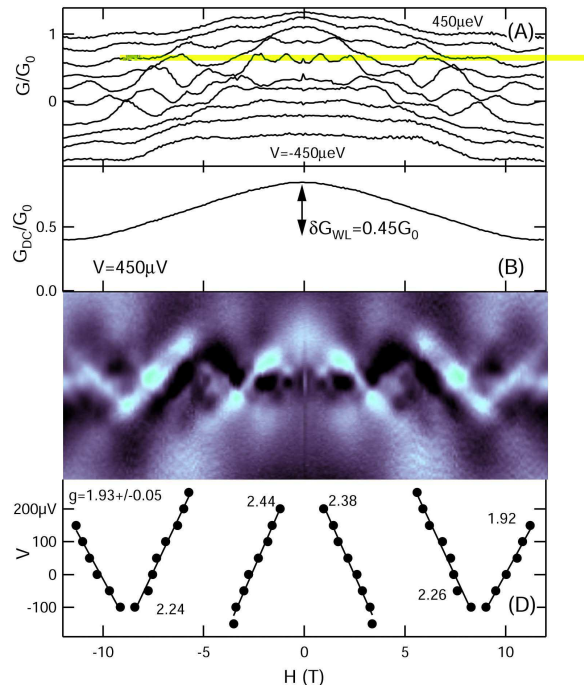


FIG. 4: A. Conductance versus Magnetic field at voltages  $-450, -350, \dots, 450\mu V$ . The lines are offset for clarity. B. Weak localization signal. C. Fluctuating conductance  $\delta G$  versus magnetic field and voltage. Voltage range  $[-450\mu V, 450\mu V]$ . Darker=smaller conductance. D. Linear fits to conductance maxima and corresponding  $g$ -factors.

In order to estimate the SO-scattering time, we need to obtain the mean free path in the leads.

To this end, we use two methods. One method consists of determining the shifts in the so-called conductance histogram peaks near  $G_0$  away from  $G_0$  [3], which estimates the resistance of the leads. In our samples, conductance histograms put a lower bound to the mean-free path. Another method can be applied to single samples. It consists of resolving a Cooper's contribution to the ZBA [1], which is highly sensitive to the applied magnetic field. The description of those methods is beyond the scope of this letter. [16]. Both methods give  $l \sim 3nm$ , within a factor of 2. This  $l$  is consistent with that found in break-junctions. [4] The SO-scattering rate in the leads, corresponding to  $l = 3nm$ , is  $\nu_{SO} \sim H_{SO} v_F l / 3\Phi_0 = 4 \times 10^{12} s^{-1}$ .

It is convenient (but unessential) to subtract the WL and the ZBA backgrounds from conductance, to obtain the fluctuating part of conductance  $\delta G(V, H) = G(V, H) - \langle G(V, H) \rangle_V - \langle G(V, H) \rangle_H + \langle G(V, H) \rangle_{V,H}$ , where  $\langle \dots \rangle_X$  indicates averaging over parameter  $X$ . The voltage and the magnetic field ranges are  $[-450\mu V, 450\mu V]$  and  $[-12T, 12T]$ , respectively.  $\delta G$  is shown in Fig. 4C.

It is striking how well the fluctuations of conductance

versus magnetic field are correlated with fluctuations of conductance versus voltage. The image in Fig. 4-C clearly indicates that there are lines in  $V-H$  space where  $G$  does not vary by much. Such lines have both positive and negative slopes. The slope magnitude varies weakly between different lines and different samples, and the lines cross with line  $V = 0$ . Circles in Fig. 4D are obtained by finding local maximums in  $G(V, H)$  using parabolic fits. Then we obtain best linear fits to  $V = \pm g\mu_B H + const$ , where  $g$  are effective g-factors (note the voltage division by 2 in Eq. 1). Some g-factors are written in Fig. 4D. In the absence of orbital effects, lines in Fig. 4C reflect addition of Zeeman energy  $\pm g\mu_B H/2$  and kinetic energy. The lines arise because the phases of wavefunctions are constant along corresponding lines.

As discussed in the introduction, Fig. 4C is analogous to an addition spectrum. The magnetic field changes the occupancy of wavefunctions of different kinetic energies, which extend through the contact. Due to surface and grain boundary scattering, the electronic wavefunctions are diffusive, and they have minima uniformly distributed throughout the leads. The positions of the minima depend on the kinetic energy (wavelength). Since magnetic field changes the kinetic energy of an electron at the chemical potential, minima migrate in response to the applied magnetic field. The ZBA is reinforced by the minima that approach the contact from the leads, explaining the nonmonotonic magnetic field dependence of the ZBA peak height.

g-factors in our samples also exhibit fluctuations, but they are weak. Averaging 11 independent g-factors in 4 samples gives  $\langle g \rangle = 2.0 \pm 0.1$  and  $rms(g) = 0.39$ . These values are consistent with average g-factor  $2.1 \pm 0.1$  in bulk gold. [10] Tunneling spectroscopy of discrete energy levels in gold nanoparticles [11, 12] find that g-factors are greatly suppressed from free-electron value.

The suppression of g-factors has been related to spin-randomization caused by SO-scattering. This effect has recently been calculated within random-matrix theory [13, 14].

The nanoparticle diameters are of the same order of magnitude as the mean free path in our leads, thus  $\nu_{SO}$  should be comparable. This suggests that SO-scattering alone is ineffective in suppressing g-factors. It appears that the g-factors are suppressed when the spectrum is discrete, and unsuppressed when the spectrum is continuous. A calculation of g-factors in small grains, as a function of the grain contact conductance, is desired.

A possible explanation for a difference in g-factors between open and isolated grains has been suggested by Matveev *et al.* [14]. Matveev *et al.* state that the effect of SO-scattering on g-factors depends on  $\delta E/\nu_{SO}$ , where  $\delta E$  is a characteristic energy scale of the system. When energy levels are discrete, then  $\delta E$  is the level spacing and g-factors can be suppressed by SO-scattering. In systems with a continuous energy spectrum, however,  $\delta E$

is the Fermi energy, and g-factors are weakly affected by SO-scattering.

In conclusion, we have discovered a zero-bias anomaly in the conductance of atomic-scale contacts between gold electrodes. The origin of this effect is puzzling, and we speculate that it is caused by an enhancement of local electron-electron repulsion. The ZBAs exhibit nonmonotonic magnetic field dependences, which we explain by the addition of the Zeeman energy and the kinetic energy. g-factors in atomic-scale contacts are consistent with g-factors in bulk gold.

This work was performed in part at the Cornell Nanofabrication Facility, (a member of the National Nanofabrication Users Network), which is supported by the NSF, under grant ECS-9731293, Cornell University and Industrial affiliates. This research is supported by the David and Lucile Packard Foundation grant 2000-13874 and the NSF grant DMR-0102960.

---

\* dragomir.davidovic@physics.gatech.edu

- [1] B. L. Altshuler and A. G. Aronov, in *Electron-Electron Interactions in Disordered Systems*, edited by A. L. Efros and M. Pollak (Elsevier and Amsterdam, 1985).
- [2] E. L. Wolf, *Principles of Electron Tunneling Spectroscopy* (Oxford University Press, 1989).
- [3] J. V. Ruitenbeek, in *Mesoscopic Electron Transport*, edited by L. L. Sohn, L. P. Kouwenhoven, and G. Schon (Elsevier and Amsterdam, 1997), p. 549.
- [4] B. Ludoph, M. Devoret, D. Esteve, C. Urbina, and J. M. van Ruitenbeek, *Phys. Rev. Lett* **82**, 1530 (1999).
- [5] D. L. Maslov, C. Barnes, and G. Kirczenow, *Phys. Rev. Lett.* **70**, 1984 (1993).
- [6] C. W. J. Beenakker and J. A. Melsen, *Phys. Rev. B* **50**, 2450 (1994).
- [7] A. Korotkov, M. Bowman, H. J. McGuinness, and D. Davidović, *cond-mat/0112235* (2001), we have modified sample fabrication since Ref [7] which improved the success of growing desirable samples.
- [8] A. I. Larkin and D. E. Khmel'nitskii, *Zh. Eksp. Teor. Fiz.* **91**, 1815 (1986), *sov. Phys. JETP* **64**, 1075, 1075 (1986).
- [9] P. A. Mello and A. D. Stone, *Phys. Rev. B* **44**, 3559 (1991).
- [10] P. Monod and A. Janossy, *J. Low. Temp. Phys.* **26**, 311 (1977).
- [11] D. Davidović and M. Tinkham, *Phys. Rev. Lett.* **83**, 1644 (1999).
- [12] J. R. Petta and D. C. Ralph, *Phys. Rev. Lett* **87**, 6801 (2001).
- [13] P. W. Brouwer, X. Waintall, and B. I. Halperin, *Phys. Rev. Lett.* **85**, 369 (2000).
- [14] K. I. Matveev, L. I. Glazman, and A. I. Larkin, *Phys. Rev. Lett.* **85**, 2789 (2000).
- [15] It is unexpected that the  $\delta G_{WL}$  in a sample with few conduction channels is well described by the maximum entropy model. We refer to the maximum entropy model corresponding to the crossover  $\beta = 4 \rightarrow \beta = 2$  within random matrix theory.
- [16] A comprehensive analysis of many samples will be pub-

lished.